TASK QUARTERLY 15 No 1, 107–119

PREPARATION, MAGNETIC STUDIES AND BAND STRUCTURE CALCULATION OF $NiFe_2O_4$ NANOPARTICLES

GHOLAMREZA NABIYOUNI[1],
MARJANEH JAFARI FESHARAKI[1]
AND ARKADIY A. ZOLOTOVSKY[2]

[1]*Department of Physics, Faculty of Science, Arak University, Shahid Beheshti Avenue, Arak 38156-8-8349, Iran*
g-nabiyouni@araku.ac.ir

[2]*Lashkaryov Institute of Semiconductor Physics, 45, Prosp. Nauky, Kiev 03028, Ukraine*

(Received 5 June 2010; revised manuscript received 10 November 2010)

Abstract: We have undertaken a comprehensive theoretical study of the band structure, density of states, dependence of the Curie point and saturation magnetization on the size of $NiFe_2O_4$ nanoparticles prepared by the conventional ceramic method. Commercially available $NiFe_2O_4$ powder was first annealed in an oxygen environment in a furnace at 1100°C for 3h. The X-ray diffraction pattern indicated that the sample was single-phase at this stage. The average grain size estimated by scanning electron microscopy (SEM) was in the range of 300 to 350nm. The magnetic behavior of the sample at room temperature was studied by means of a superconducting quantum interference device (SQUID). The Curie temperature of the nickel ferrite powder was measured using an LCR meter. The measurement of the Curie temperature and saturation magnetization indicated that a decrease in the grain size leads to a decrease in the Curie temperature and in the saturation magnetization. The small value of saturation magnetization was attributed to a spin-glass-like surface layer on the nanocrystalline nickel ferrite with a ferrimagnetically aligned core [1]. Good agreement was obtained between theory and experimental results.

Keywords: band structure calculation, nickel ferrite nanopowder, Curie temperature, spin-glass

1. Introduction

There is a growing interest in magnetic ferrite nanoparticles, owing to their wide applications in permanent magnets, magnetic drug delivery, microwave devices [2] and high-density information storage technology [3, 4]. Spinel ferrites have the general molecular formula $(A^{2+})\ [B_2^{3+}]\ O_4^{2-}$, where A^{2+} and B^{3+} are

divalent and trivalent cations, respectively, occupying the tetrahedral (A) and octahedral (B) interstitial positions of the fcc lattice formed by O^{2-} ions. Nickel ferrite ($NiFe_2O_4$) is an inverse spinel in which the tetrahedral or A-sites are occupied by ferric ions, and the octahedral or B-sites – by ferric and nickel ions. Thus, the compound can be represented by the formula: $(Fe^{3+})[Ni^{2+}Fe^{3+}]O_4^{2-}$. The magnetic structure is generally assumed to be of the Néel collinear type, *i.e.* the magnetization of the A sublattice is antiparallel to that of the B sublattice [5].

This material is widely used in electric and electronic devices, as well as in catalysis [6, 7]. In the present study, we investigated the synthesis of nanocrystalline $NiFe_2O_4$ powders using the conventional ceramic method by annealing the powders at high temperature (1100°C). The Curie temperature, saturation magnetization and hysteresis (M-H) loops as a function of powder grain size were investigated. In the theoretical calculations, the renormalization group method is applied to investigate the Curie temperature and magnetization. The experimental results and theoretical calculations are compared and dependence of the Curie temperature and magnetization to the particle sizes are studied. Finally the band structure and density of states (DOS) are calculated for Nickel ferrite using Pickett and Hohenberg-Kohn DFT.

2. Experiment

Polycrystalline nickel ferrite was first synthesized by the conventional ceramic method. In order to produce nickel ferrite ($NiFe_2O_4$), nickel oxide (Ni_2O_3) and iron oxide (Fe_2O_3) were mixed at a molar ratio of 1 : 2 ($Ni_2O_3 + 2Fe_2O_3 \rightarrow NiFe_2O_4 + 1/2O_2$). This was followed by annealing the mixture in an oxygen environment in a furnace at 1100°C for 3 h.

In order to investigate the formation of a nickel ferrite phase in the powder, the structure of the sample was studied by X-ray diffraction and the average grain size was estimated by scanning electron microscopy (SEM). The obtained nickel ferrite was then milled in a steel cylinder of a SPEX high-energy shaker mill for 10 h. The mill cylinder was loaded with 10 g of $NiFe_2O_4$ (with a purity of 99.95 at. %) and 30 g of steel balls. The mill was set to shake at a frequency of *ca.* 1200 Hz. The milled sample was annealed at 500°C for 5 h. The Curie temperature of the samples was measured by an LCR meter. The measurements of magnetic properties and magnetization were performed using a superconducting quantum interference device (SQUID) magnetometer. The hysteresis (M-H) loops of the samples were studied.

2.1. Crystal structure

Figure 1 shows the XRD pattern of the sample prepared by the conventional ceramic method. Several strong and sharp peaks attributed to the face-centered cubic $NiFe_2O_4$ phase with a lattice constant of 8.33 Å are visible [8]. The SEM image of a similar sample (Figure 2) illustrates the general morphology and indicates the high yield of the $NiFe_2O_4$ octahedron phase. The octahedron faces

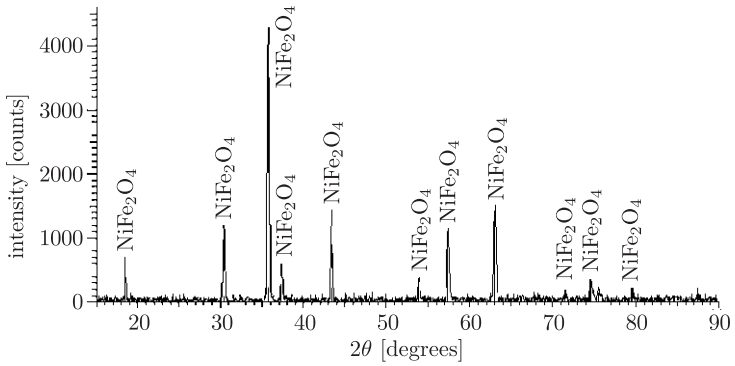

Figure 1. X-ray diffraction pattern of $NiFe_2O_4$ powder sample prepared by the conventional ceramic method

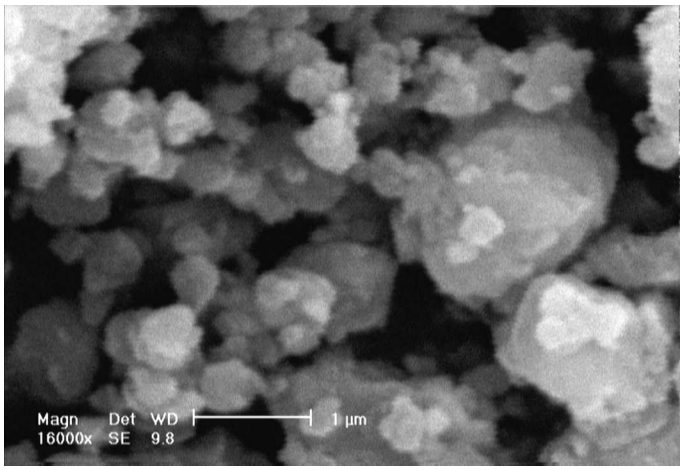

Figure 2. Scanning electron microscopy image of $NiFe_2O_4$ powder sample prepared by the conventional ceramic method

can be distinguished. The size distribution of the octahedra ranges from 300 to 350 nm.

2.2. Curie temperature measurement

The measurements of Curie temperatures for both bulk and nanocrystalline nickel ferrites were performed with an LCR meter. The results are shown in Figures 3 and 4, respectively. The Curie temperature of nanocrystalline nickel ferrite was lower than that of the bulk material (Figures 3 and 4). A decrease in inductance with an increase in temperature can be explained on the basis of Néel theory [9]. In fact, the intrinsic magnetization vanishes at the Curie temperature, therefore, the smaller the size of the particle, the lower the Curie temperature.

2.3. Magnetization measurement

The magnetization curve as a function of the applied magnetic field was obtained with a SQUID magnetometer (Figure 5).

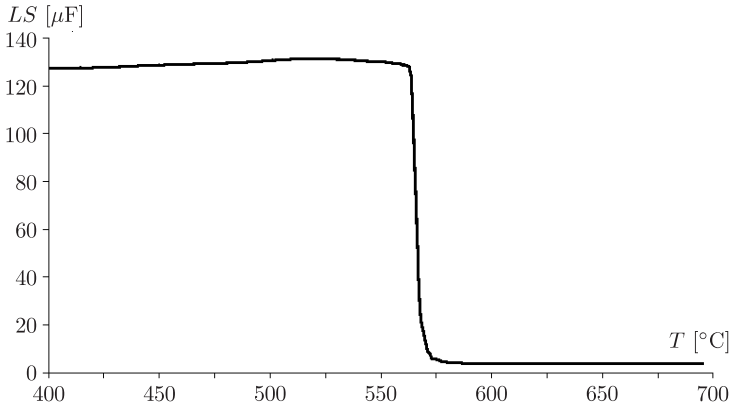

Figure 3. Inductance versus temperature for bulk $NiFe_2O_4$. The Curie temperature was measured to be 570°C

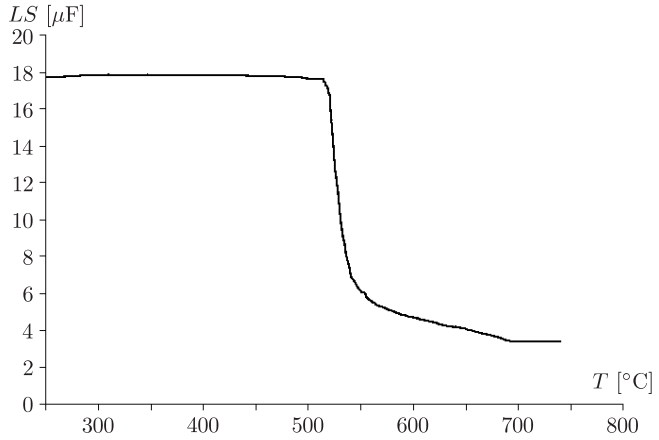

Figure 4. Inductance versus temperature for nanocrystalline $NiFe_2O_4$. The Curie temperature was measured to be 517°C

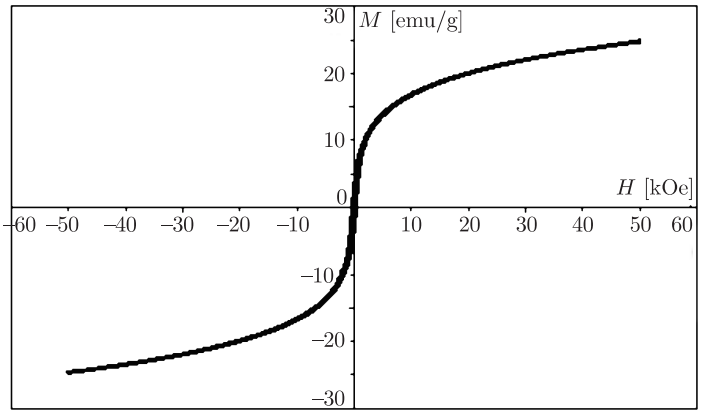

Figure 5. Magnetization versus the applied magnetic field

The saturation magnetization of nanocrystalline $NiFe_2O_4$ at 300K was measured to be 24emu/g. This value was significantly lower than 55emu/g reported for multidomain bulk $NiFe_2O_4$ [10]. The small value of saturation magnetization (as compared with that measured for multidomain bulk $NiFe_2O_4$) has been recently explained in terms of the core-shell morphology of nanoparticles consisting of ferrimagnetically aligned core spins and a spin-glass-like surface layer [1]. If this surface layer was absent, the saturation value of magnetization of the particles would increase with the applied magnetic field up to a particular magnetic field, whereas the core magnetic moments would be aligned in the applied field. Nanoparticles which have a large surface-to-volume ratio exhibit enhanced spin disorder in contrast to large (micron-size) particles when the magnetizations are measured in the same applied magnetic field and at the same temperature [1]. The magnetic moment anomalies of the surface layer can be attributed to broken exchange bonds, the high-anisotropy layer on the surface, or to the loss of the long-range order in the surface layer. These effects are more pronounced in the case of ferrites because of the superexchange interactions between the oxygen ions. The presence of another atom (ion) in the form of impurity or the absence of oxygen ions on the surface leads to the breakage of superexchange bonds between magnetic cations, inducing a large surface spin disorder [11]. The superexchange interaction depends on the bond angles and bond lengths, which would be different on the surface due to the termination of bonds [12].

3. Theoretical calculations

3.1. Band structure and density of states (DOS)

The bands were calculated using the method outlined by Pickett [13], and by Hohenberg-Kohn DFT [14]. A summary of the method and its applications was presented by Devreese and Van Camp [15], therefore the method is only outlined here.

Starting with the N-electron problem in the field of ionic potentials:

$$V_{\text{ion}}(r) = \sum_m v_{\text{ion}}(r - \boldsymbol{R}_m) \tag{1}$$

with the ions fixed at positions $\boldsymbol{R}_m$, we have the Hamiltonian:

$$H = \sum_i \frac{p_i^2}{2m} + \int n(r) V_{\text{ion}}(r) dr + \frac{1}{2} \iint n(r) v(r - r') n(r') dr dr' \tag{2}$$

where $n(r)$ is the electronic density at r and $v(r-r')$ is the Coulomb interaction. Hohenberg and Kohn established that there is a one-to-one correspondence between the ionic potential V_{ion} (to within an arbitrary constant) and the ground state density n, and therefore the many-body problem can be considered as a functional of the density rather than as a functional of the potential [14]. Hohenberg and Kohn established that for variations δn of the energy density which conserve the particle number N, the ground-state energy functional $E[n]$

is minimized by the ground-state density, with corrections of order δn^2. The resulting variational principle allows one to accurately obtain numerical results. Kohn and Sham [16] recast the energy functional into the form:

$$E[n] = T_0[n] + \int V_{\text{ion}}(r)n(r)dr + \frac{1}{2}\iint n(r)v(r-r')n(r')drdr' + E_{\text{xc}}[n] \quad (3)$$

where $T_0[n]$ is the kinetic energy of the system of non-interacting electrons with the same density $n(r)$, and the exchange-correlation energy $E_{\text{xc}}[n]$ is defined by this expression (3). If one has adequate approximations for $T_0[n]$ and $E_{\text{xc}}[n]$, the energy can be obtained directly from Equation (3) by minimizing the energy with respect to $n(r)$. $T_0[n]$ can be obtained exactly from the kinetic energies of the one-particle wave-functions:

$$\left[\frac{p^2}{2m} + V_{\text{eff}}(r; n)\right]\psi_i(r) = E_i\psi_i \quad (4a)$$

$$V_{\text{eff}}(r; n) = V_{\text{ion}}(r) + \int v(r-r')n(r')dr' + v_{\text{xc}}(r; n) \quad (4b)$$

$$n(r) = \sum_i^{\text{occ}} |\psi_i(r)|^2 \quad (4c)$$

where

$$v_{\text{xc}}(r; n) = \frac{\delta E_{\text{xc}}[n]}{\delta n}(r) \quad (5)$$

The energy functional is minimized by the density functional described by these equations, and the energy is obtained by iteration to self-consistency. Within density-functional theory, the one-electron eigenvalues and eigenfunctions have no physical meaning, and are not physically realizable. They are the true excitation energies and eigenfunctions of the system of non-interacting electrons, which has the same density as the interacting material of interest; they arise from the „external" potential V_{eff}. This system is not physically realizable, but has an interesting connection to the excitations. When well-defined quasi-particles exist (*i.e.*, their widths are much less than their energies), they are described by the non-Hermitian problem:

$$\left(\frac{p^2}{2m}\right)\psi_i(r, E_i) + \int M(r, r', E_i)\psi_i(r', E_i)dr' = E_i\psi_i(r) \quad (6)$$

This equation bears a formal resemblance to the Kohn-Sham eigenvalue equation (4a). In many solids, angle-resolved photoemission studies have shown that the bands from Equation (4a) bear a close resemblance to the single-particle excitations in the region of the fundamental band gap. The self-energy is well represented by a local, real, energy-independent, effective potential V_{eff}. Conversely, when the excitations do not correspond directly to the calculated bands, one can conclude that the non-locality or energy-dependence of the self-energy is necessary for an understanding of the excitations. The lack of correspondence between calculated bands and observed excitations does not in itself invalidate the formalism for

obtaining ground-state properties. The exchange-correlation functional $E_{\mathrm{xc}}[n]$ remains unknown. The large majority of calculations invokes the highly successful local-density approximation.

$$E_{\mathrm{xc}}[n] = \int \varepsilon_{\mathrm{xc}}(n(r))n(r)dr \tag{7}$$

where $\varepsilon(n)$ is the exchange-correlation energy-density of the homogeneous interacting electron gas of density n, which is known. Reviews containing discussions of applications of density functional theory and of the generalization to spin-polarized systems are given, for example, in the book by Devreese and Van Camp [15]. The results of calculations of the band structure and the density of states for $NiFe_2O_4$ are presented in Figure 6.

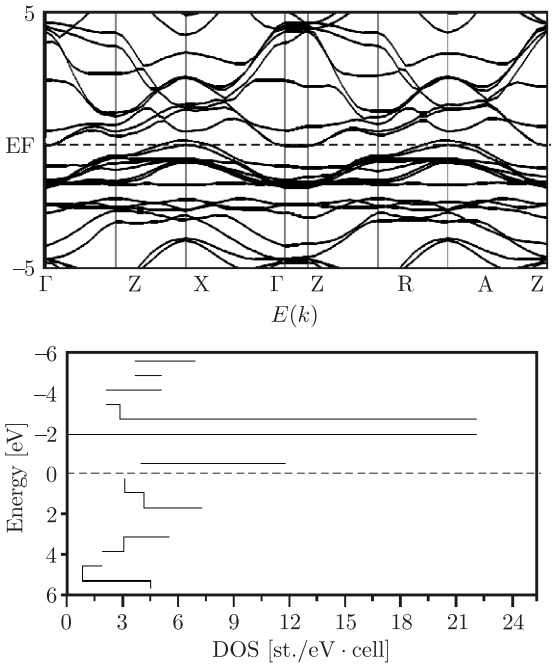

Figure 6. Results of our calculations of the band structure and the density of states (DOS) for $NiFe_2O_4$

From the shape of the partial density of states it follows that the density of states near the Fermi level is in practice completely determined by the d-states of Fe (with rather insignificant contribution of the p-states of O).

3.2. Curie point and saturation magnetization

The renormalization group method was applied to the investigation of the dependence of the Curie point and saturation magnetization on the size of nanoparticles. Previously, the renormalization group method (scaling) was used only for bulk crystals (infinite lattice). For the infinite lattice, two parameters were introduced: the correlation radius r_c and the size r_0 of the solid section, in which

the mean-square fluctuation was compared with its characteristic equilibrium value. In the nanoparticle, which consists of one domain, the correlation radius r_c was compared with the lattice size. Theoretical estimations and their comparison with experiment showed that the renormalization group method was applicable to nanoparticles. Section 4 describes the critical point exponents typical of a second-order phase transition. Section 5 describes the dependence of the Curie point and saturation magnetization on the size of the nanoparticles obtained by the renormalization group method.

4. Thermodynamic functions and critical behavior

For systems where the interactions are short-ranged, isotropic coupling, *i.e.* the interaction Hamiltonian [17] was introduced:

$$H\{\vec{s}_x\} = H_{\text{iso. exch.}} = -\frac{1}{2}\sum_{x,\,x'} J(x-x')\vec{s}_x \cdot \vec{s}_{x'} \tag{8}$$

Let us consider a ferromagnet in equilibrium at temperature T and under the action of a uniform magnetic field H. We will use the reduced temperature [18]:

$$t = \frac{T - T_C}{T_C} \tag{9}$$

where T_C is the critical temperature (or Curie, or Néel point) and consider properties as $\to 0$ with $H = 0$. In this regime, the initial susceptibility diverges as [19]:

$$\chi_0(T) \approx \frac{C}{t^\gamma} \tag{10}$$

The specific heat in zero field displays a critical anomaly which may be characterized by:

$$C_{H=0}(T) \approx \frac{A}{t^\alpha} \tag{11a}$$

or, more usefully in practice, by:

$$C_{H=0}(T) \approx \tilde{A}\frac{t^{-\alpha} - 1}{\alpha} \tag{11b}$$

Classical theory predicts only a jump discontinuity in $C(T)$. The scaling theory of critical behavior now asserts that the singular part of the free energy $F(T, H)$ varies asymptotically as:

$$f(T,H) = -(k_B T)^{-1} F_{\text{sing}}(T,H) \approx t^{2-\alpha} Y \frac{H}{t^\Delta} \tag{12}$$

where the gap exponent Δ is determined in terms of α and γ by:

$$\Delta = \frac{1}{2}(2 - \alpha + \gamma) \tag{13}$$

For a fluid the magnetic field H is to be replaced by the chemical potential difference $\mu - \mu_\sigma(T)$, where $\mu_\sigma(T)$ is the value on vapor pressure curve and its linear extension [19]. The scaling function $Y(y)$ depends only on a single variable,

but is not otherwise given explicitly by the theory. From Equation (11b) we find the spontaneous magnetization vanishes when $t \to 0$ as:

$$M_0(T) \approx B|t|^{\beta} \tag{14a}$$

where the exponent is predicted by the exponent relation:

$$\beta = \frac{1}{2}(2 - \alpha - \gamma) \tag{14b}$$

In addition, it follows that the equation of state $M = M(T, H)$ can be written asymptotically in the reduced or scaled form:

$$\frac{M}{t^{\beta}} \approx W\frac{H}{t^{\Delta}} \tag{15}$$

where $W(y)$ is again a single-variable scaling function.

In addition to thermodynamic behavior, the variation of the scattering intensity with wave vector $\boldsymbol{q}$, and temperature, is of particular interest in the critical region. This is proportional to:

$$\widehat{G}(\boldsymbol{x}, T) = \sum_{\boldsymbol{x}} \exp(i\boldsymbol{q}\cdot\boldsymbol{x})G(\boldsymbol{x}, T) \tag{16}$$

where the basic two-point correlation function is:

$$G(\boldsymbol{x}, T) = \left\langle \vec{S}_0 \cdot \vec{S}_{\boldsymbol{x}} \right\rangle \tag{17}$$

in which $\vec{S}_{\boldsymbol{x}}$ denotes a (localized) spin at site $\boldsymbol{x}$. At the critical point itself, one has:

$$\begin{aligned} &G_C(\boldsymbol{x}) \approx \frac{D_C}{x^{d-2+\eta}}, \quad \text{or} \quad \widehat{G}(\boldsymbol{q}) \approx \frac{\widehat{D}_C}{q^{2-\eta}}, \\ &\text{as} \quad x \to \infty, \qquad\qquad \text{or} \quad q \to 0 \end{aligned} \tag{18}$$

As $t \to 0$ (in ero field) scaling predicts the form:

$$G(x, T) \approx x^{-d+2-\eta} D\left(\frac{x}{\xi}\right), \quad \xi \sim t^{-\nu} \tag{19}$$

where ξ is the correlation length or, equivalently:

$$\widehat{G}(\boldsymbol{q}, T) \approx Ct^{-\gamma}\widehat{D}\frac{q^2}{t^{2\nu}} \tag{20}$$

The correlation length exponent is given by:

$$\nu = \frac{\gamma}{2-\eta} \tag{21}$$

The scaling function $\widehat{D}(z^2)$ represents the scattering „line shape" near T_C. When $\eta > 0$, it must necessarily deviate from a simple Lorentzian (or OZ, Ornstein-Zernike) form close to the critical point, although this may be hard to detect.

The exponent for the critical isotherm δ:

$$H \sim M^{\delta} \tag{22}$$

the lattice sites will have coordinate vectors $\boldsymbol{x} = (x_i)$ with $i = 1, 2, \ldots d$, where d is the spatial dimensionality. By habit we normally consider only $d = 3$, 2 and 1. It will turn out later that, having defined continuous d, the difference:

$$\varepsilon = 4 - d \tag{23}$$

forms a natural and important small parameter.

Once we have a lattice with sites $\boldsymbol{x}$, we must populate it with spins $\vec{S}_{\boldsymbol{x}}$. We suppose the spin vector has n components, *i.e.* $\vec{S}_{\boldsymbol{x}} = (S_x^{\mu})$ with $\mu = 1, 2, \ldots n$, which enter equally into interactions. The basic cases for the symmetry index are:

(a) $n = 3$, ordinary or Heisenberg spins, $\vec{S} = (S^x, S^y, S^z)$;

(b) $n = 2$, XY or „planar" spins, $\vec{S} = (S^x, S^y)$;

(c) $n = 1$, uniaxial or Ising spins, $\vec{S} = S^z$.

The last, Ising-like case also describes classical density fields as appropriate to fluids, alloys, *etc.* The $n = 2$ or XY-like case includes quantal fields since the wave function $\Psi = (\Psi', \Psi'')$ has independent but equivalent, real and imaginary components.

One exponent scaling relation remains:

$$d\frac{\delta - 1}{\delta + 1} = 2 - \eta \tag{24}$$

One of the most important outputs of the practical renormalization group calculations has been expansions for the critical exponents. In leading order in ε (> 0) the deviations from classical behavior for systems with isotropic short range exchange are revealed by:

$$\begin{aligned}\gamma = 1 + \frac{(n+2)}{2(n+8)}\varepsilon + \frac{(n+2)(n^2+22n+52)}{4(n+8)^3}\varepsilon^2 + \frac{(n+2)}{8(n+8)^3}\Bigg[(n+2)^2 + \\ 24\frac{(n+2)(n+3) - (10n+44)\zeta(3)}{(n+8)} + 4\frac{55n^2+268n+424}{(n+8)^2}\Bigg]\varepsilon^3 + O(\varepsilon^4)\end{aligned} \tag{25}$$

$$\beta = \frac{1}{2} - \frac{3}{2(n+8)}\varepsilon + \ldots \tag{26}$$

$$\alpha = \frac{4-n}{2(n+8)}\varepsilon + \frac{(n+2)^2(n+28)}{4(n+8)^3}\varepsilon^2 + \ldots \tag{27}$$

$$\begin{aligned}\eta = \frac{n+2}{2(n+8)^2}\varepsilon^2 + \frac{n+2}{8(n+8)^2}\left[\frac{24(3n+14)}{(n+8)^2} - 1\right]\varepsilon^3 + \frac{n+2}{2(n+8)^2}\Bigg[\frac{-5n^2+234n+1076}{16(n+8)^2} - \\ 8\frac{3n^2+53n+160+3(5n+22)\zeta(3)}{(n+8)^2} + 45\frac{(3n+14)^2}{(n+8)^4}\Bigg]\varepsilon^4 + O(\varepsilon 5)\end{aligned} \tag{28}$$

$$\delta = 3 + \varepsilon + \ldots \tag{29}$$

where $\zeta(3) = \sum_{k=1}^{\infty} \frac{1}{k^3} \approx 1.2020569$ (Riemann function).

5. Discussion

Nickel ferrite ($NiFe_2O_4$) is an inverse spinel, which has a three-dimensional structure: $d=3$, $\varepsilon=4-d=1$. It was assumed that for the three-dimensional Heisenberg spin, $n=3$. During the investigation of a second-order phase transition by the scaling approach, in the case of bulk crystals two characteristic sizes were used, which determine the space distribution of fluctuations – the correlation radius r_c and the size r_0 of the solid section, in which the mean-square fluctuation of the order parameter was compared with its characteristic equilibrium value. The condition for the applicability of the Landauer theory is $r_c >> r_0$. For $t \to 0$, an increase in r_0 is more substantial than in r_c, whereas on the boundary of the Landauer regime they are equal. From the theoretical point of view, the most important assumption about the fluctuation regime (*i.e.* everywhere $r_0 \sim r_c$) is that: within this regime the small parameter is practically absent [20]. For nanoparticles, r_0 corresponds to their characteristic size. A nanoparticle can be considered as one domain. In the case of the bulk crystal it can be assumed that the sizes are infinite and thus the surface effects can be neglected, however, in the case of nanoparticles, the finite size should be taken into account. The Curie point of the bulk crystal was denoted with T_{c_0}. The Curie point of the nanoparticle was lower than that of the bulk crystal: $T_c < T_{c_0}$. This can be explained by the exchange interactions between O^{2-} ions and by the strain of bonds on the boundary of the nanoparticle, which destroys the spin correlation. In nanoparticles T_{c_0} plays the role of the usual temperature. The results obtained for the critical exponents were as follows:

$$\begin{aligned} &\alpha = 0.19102,\ \beta = 0.23121,\ \gamma = 1.34656,\ \eta = 0.03161, \\ &\Delta = 1.57777,\ \nu = 0.68409,\ \delta = 4.81615 \end{aligned} \tag{30}$$

It was assumed that the size of the nanoparticles was 10 nm. Using the results from [21, 22] as a starting point, the Curie temperatures and dependences of magnetization due to the magnetic field, as calculated by the renormalization group method for the nanoparticles, are presented in Figures 7–9. The results are in good agreement with experimental data.

6. Conclusions

Nanocrystalline nickel ferrite was synthesized using the conventional ceramic method and exhibited a Curie temperature of 517°C.This value was lower than that obtained for bulk nickel ferrite (570°C). A decrease in the saturation magnetization of the magnetic nanocrystalline nickel ferrite, as compared with the bulk ferrite, can be explained in terms of a two-component nanoparticle system consisting of a spin-glass-like surface layer and a ferrimagnetically aligned core. Theoretical calculations, performed by the renormalization group method (scaling), also predict the Curie temperature of the nanoparticles to be lower than that of the bulk crystal. This can be explained by the presence of exchange interactions

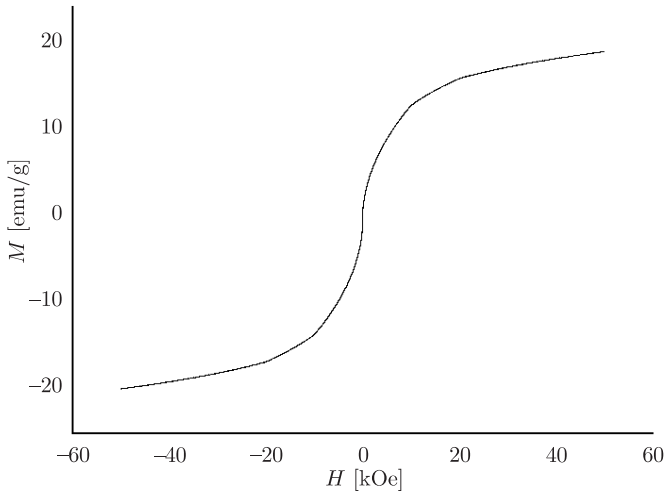

Figure 7. Dependence of magnetization on the magnetic field strength for the nanoparticles with size of 5nm, $T_c = 424.01°\mathrm{C}$

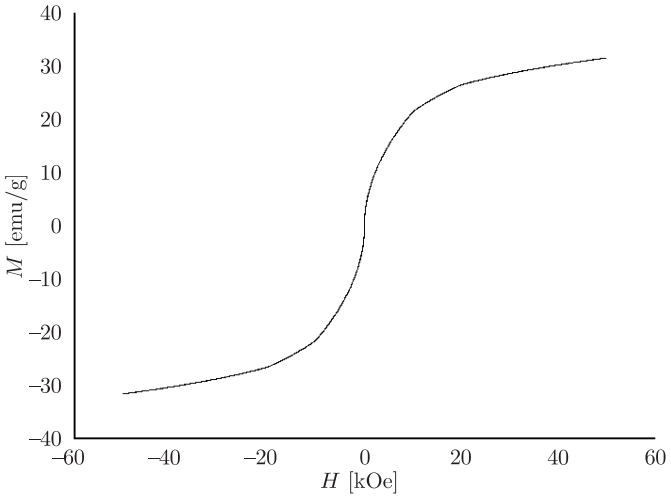

Figure 8. Dependence of magnetization on the magnetic field strength for the nanoparticles with size of 20nm, $T_c = 550.76°\mathrm{C}$

between O^{2-} ions and by the strain of bonds on the boundary of the nanoparticle, which destroys the spin correlation. The dependence of magnetization on the magnetic field strength for the nanoparticles (5, 20 and 50nm in size) shows that a decrease in the grain size leads to a decrease in the magnitude of the saturation magnetization. The theoretical calculations were in good agreement with experimental data.

References

[1] Nathani H and Gubbala S 2004 *J. Mater. Sci. and Engin. B* **111** 95
[2] Mo N, Young-Yeal Song and Patton C E 2005 *J. Appl. Phys.* **97** 93901

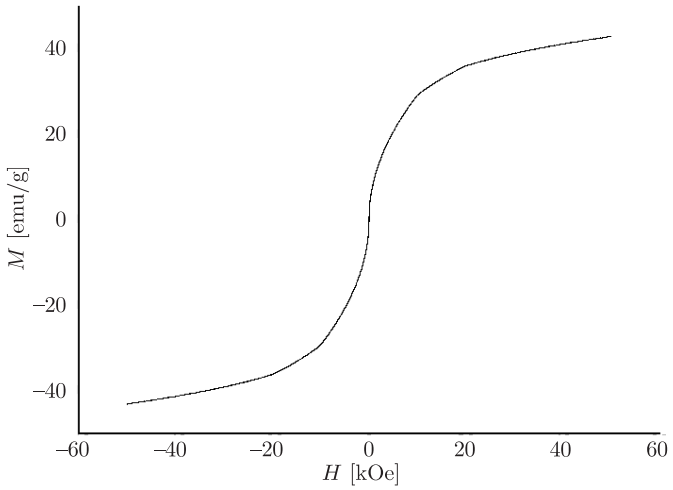

Figure 9. Dependence of magnetization on the magnetic field strength for the nanoparticles with size of 50nm, $T_c = 564.96°\mathrm{C}$

[3] Lee S, Drwiega J, Mazysk D and Wu Ch 2006 *J. Mater. Chem. Phys.* **96** 2
[4] Gabal M A and Alangari Y M 2009 *J. Mater. Chem. Phys.* **115** 578
[5] Mo N, Young-Yeal Sang and Patton C E 2005 *J. Appl. Phys.* **97**
[6] Rezlescu E, Iftimite N and Popa P D 2005 *J. Appl. Phys.* **15** 51
[7] Satyanarayana L and Madhusudan Reddy K 2003 *J. Mater. Chem. Phys.* **82** 21
[8] Wang Yi, Tlan Y and Zhang Ch 2008 *J. Mater. Sci. Technol.* **24** 419
[9] Morrish A H 2002 *The Physical Principles of Magnetism*, Wiley-Interscience, New York
[10] Smit J and Wijn H P J 1959 *Ferrites, Physical Properties of Ferromagnetic Oxides in Relation to Their Technical Applications*, Wiley, New York
[11] Misra R D K and Kale A 2003 *J. Mater. Sci. Technol.* **19** 826
[12] Caizer C and Stefanescu M 2002 *J. Phys. D: Appl. Phys.* **35** 3035
[13] Kohn W 1986 *Phys. Rev. B* **33** 4331
[14] Hohenberg P and Kohn W 1964 *Phys. Rev.* **136** 864
[15] Patashinskii A Z and Pokrovskii V L 1964 *Zh. Teor. Eksp. Fiz.* **46** 994
[16] Kohn W and Sham L 1965 *J. Phys. Rev.* **140** 1133
[17] Wilson K G 1971 *Phys. Rev. B* **4** 3174
[18] Fisher M E 1974 *Rev. Mod. Phys.* **46** 597
[19] Wilson K G and Kogut J 1974 *Phys. Rept.* **12C** 75
[20] Kadanoff L P 1966 *Physics* **2** 263
[21] Hasmoney E and Depeyrot J 2000 *J. Appl. Phys.* **88** 6628
[22] Caiser C and Stefanescu M 2002 *J. Phys. D: Appl. Phys.* **35** 3035